Available online at www.sciencedirect.com
ScienceDirect
Journal of Sound and Vibration 324 (2009) 832–849
JOURNAL OF SOUND AND VIBRATION
www.elsevier.com/locate/jsvi

# Analytical piezoelasticity solution for vibration of piezoelectric laminated angle-ply circular cylindrical panels

S. Kapuria*, P. Kumari, J.K. Nath

*Department of Applied Mechanics, Indian Institute of Technology Delhi, New Delhi 110016, India*

Received 2 August 2008; received in revised form 16 December 2008; accepted 21 February 2009
Handling Editor: L.G. Tham
Available online 27 March 2009

**Abstract**

An exact two-dimensional (2D) piezoelasticity solution is presented for free vibration and steady-state forced response of simply supported piezoelectric angle-ply laminated circular cylindrical panels in cylindrical bending under harmonic electromechanical load, with and without damping. The piezoelectric layers are polarized along radial direction to induce extension actuation/sensing mechanism. The variables are expanded layerwise in Fourier series to satisfy the boundary conditions at the simply supported ends. The governing equations get reduced to ordinary differential equations in thickness direction with variable coefficients and these are solved by the modified Frobenius method. The unknown coefficients of the solution are obtained using the transfer matrix method. Results for the natural frequency and its variation with ply angle and for steady-state response due to harmonic electromechanical excitation are presented for single layer piezoelectric panel, and hybrid multilayered inhomogeneous test, composite and sandwich panels. The numerical results presented in tabular form would serve as useful benchmark for assessing one-dimensional (1D) panel theories for free vibration and harmonic response of hybrid cylindrical panels.


## 1. Introduction

The development of light weight smart plate/shell type structures made up of advanced composite and sandwich materials with distributed piezoelectric sensor and actuator layers surface bonded or embedded in it has great potential for use in the new generation of aerospace, automobile, ship and space structural applications. Exact analytical solutions of coupled field equations of three-dimensional (3D) piezoelasticity with the exact satisfaction of the boundary and interface conditions of such so-called hybrid laminated structures are immensely useful for assessing the accuracy of the two-dimensional (2D) plate and shell theories and one-dimensional (1D) beam theories that are developed for efficient analysis of these structures. This need has led to the development of a number of exact 3D piezoelasticity solutions for hybrid plates and shells of various geometries under different loading conditions [1]. Exact 3D piezoelasticity solutions for simply supported rectangular cross-ply hybrid piezoelectric plates have been developed for static electromechanical

*Corresponding author. Tel.: +91 11 2659 1218; fax: +91 11 2658 1119.
*E-mail address:* kapuria@am.iitd.ac.in (S. Kapuria).

0022-460X/$ - see front matter © 2009 Elsevier Ltd. All rights reserved.
doi:10.1016/j.jsv.2009.02.035

[2,3], static thermal [4,5], free vibration [6], forced vibration [7] and buckling [8] response. Exact 2D solutions for the generalized plane strain problems of piezoelectric and magnetoelastic angle-ply flat panels in cylindrical bending have been presented for static electrothermomechanical response [9] and steady-state forced harmonic response [10]. For these laminates, the governing equations for each layer are reduced to a set of ordinary differential equations (ODEs) in the thickness coordinate with constant coefficients, which are solved analytically.

Exact piezoelasticity [11] and piezothermoelasticity [12] solutions for static response of simply supported infinite cross-ply piezoelectric circular cylindrical panels have been presented, wherein the governing equations are reduced to a set of second-order ODEs of Euler–Cauchy type, which are solved exactly. Exact piezoelasticity solutions for static [13] and free vibration [14] response of axially polarized transversely isotropic piezoelastic finite-length circular cylindrical shells have been obtained by using potential function method and expressing the solution in terms of Bessel functions. For simply supported finite-length cross-ply cylindrical shells and angle-ply infinite cylindrical panels, the governing equations of piezoelasticity reduce to first-order ODEs of variable coefficients, which pose difficulty in obtaining an exact analytical solution. Chen and Shen [15,16] employed power series method to obtain the 3D piezoelasticity solution for static axisymmetric and free vibration response of hybrid circular cylindrical shells. In both cases, however, the piezoelectric constants considered for radial poling direction are inconsistent with the elastic constants. Kapuria et al. [17,18], and Xu and Noor [19] presented 3D piezothermoelasticity solutions for static response of cross-ply finite circular cylindrical shells and panels using an elegant modified Frobenius method which yields faster convergence compared to the conventional Frobenius and power series methods. A similar solution for the static electrothermomechanical response of simply supported angle-ply hybrid cylindrical panels in cylindrical bending has been presented by Dumir et al. [20]. Chen and Lee [21] have presented an approximate analytical 2D solution for static and free vibration response of elastic angle-ply laminated cylindrical panels by employing a layerwise method. In this method, each layer of the laminate is divided into a number of sublayers and variable coefficients of the governing differential equations are approximated to be constants with their values corresponding to the middle surface of the sublayer. The same method was applied for the 3D piezoelasticity solution of cross-ply hybrid finite circular cylindrical panels [22], but the piezoelectric layers are considered to be axially polarized giving rise to the shear actuation mechanism ($d_{24}$ effect) and not the extension actuation mechanism ($d_{31}/d_{32}$) effect, that is required for effective actuation and sensing in structural applications. No results were presented for response due to electric potential load. Ootao and Tanigawa [23] obtained the quasi-static piezothermoelastic response under transient thermal loading for simply supported angle-ply hybrid radially polarized circular cylindrical panels in cylindrical bending. They reduced the governing ODEs with variable coefficients to those with constant coefficients by employing the variable substitution method. A similar method was adopted by Chen and Lee [24] to obtain the static electromechanical response of simply supported infinite-length angle-ply hybrid shells featuring weak interfaces, for which no results were presented for the electric potential loading case. The variable substitution method, however, does not lead to constant coefficients in ODEs for the dynamic case. To the best of the authors' knowledge, no exact analytical solution exists for the free and forced vibration response of angle-ply hybrid radially polarized piezoelectric cylindrical panels. The present work is aimed to fill up this void in the literature.

The objective herein is to present analytical exact 2D piezoelasticity solutions for free vibration response and steady-state harmonic response of simply supported hybrid radially polarized piezoelectric angle-ply cylindrical panels under electromechanical excitation with damping. The basic entities in this generalized plane strain problem for each layer are expanded in Fourier series in the span coordinate to satisfy the boundary conditions at the simply supported ends. The governing equations reduce to first-order ODEs with variable coefficients in the thickness coordinate. These are solved by the modified Frobenius method, wherein the solution is constructed as a product of an exponential function and a power series. The momentum and charge balance equations yield a linear eigenvalue problem for the exponent of the exponential term with eight eigenvalues and eigenvectors and a recursive relation for the coefficients of the power series. The general solution for each layer is expressed in terms of the values of the eight primary variables at the bottom of the layer. Using the continuity conditions at the layer interfaces, a laminate transfer matrix is built which relates the eight primary variables at the top and bottom surfaces. These are finally computed from the boundary

conditions at the top and bottom. Since piezoelasticity equations are used, the exact solutions presented are valid for shallow and deep shell panels. Benchmark results are presented for natural frequency and steady-state harmonic response of single layer piezoelectric panel and multilayered angle-ply piezoelectric test, composite and sandwich cylindrical panels.

## 2. Governing equations

Consider an infinitely long, simply supported, angle-ply laminated hybrid circular cylindrical panel (Fig. 1) with span angle $\psi$ along the circumferential direction $\theta$, thickness $h$ in the radial direction $r$, made up of $L$ perfectly bonded layers. The panel is subjected to electromechanical harmonic load which is independent of the axial coordinate $z$. The layers can be orthotropic elastic with a principal material axis along the radial direction or piezoelectric with orthorhombic class mm2 symmetry with poling in the direction of principal material axis in the radial direction. The mean radius of the panel is $R$ and its inner and outer radii are $R_i, R_o = R \mp h/2$, respectively. Let the thickness and the inner radius of the $k$th layer (numbered from inside) be $t^{(k)}$ and $R_1^{(k)}$. Let the angle made by its fiber axis with the $\theta$-axis in $\theta z$ plane be $\beta^{(k)}$. The interface between the $k$th and $(k+1)$th layers is named as the $k$th interface with $r = R_1^{(k+1)}$. Henceforth the layer superscript is omitted for clarity unless needed. The simple supports at $\theta = 0, \psi$ are electrically grounded and are modeled such that the supports prevent only the radial displacement $u$, i.e. the tractions along directions $\theta$ and $z$ are zero. The displacements $v, w, u$ are taken in $\theta, z, r$ coordinate directions. All response entities, namely, displacements $v, w, u$; electric displacements $D_\theta, D_z, D_r$; electric potential $\phi$; electric field $E_\theta, E_z, E_r$; strains $\varepsilon_\theta, \varepsilon_z, \varepsilon_r, \gamma_{zr}, \gamma_{r\theta}, \gamma_{\theta z}$; and stresses $\sigma_\theta, \sigma_z, \sigma_r, \tau_{zr}, \tau_{r\theta}, \tau_{\theta z}$, are independent of $z$.

The strain–displacement relations and the electric field-potential relations for this generalized plane strain are given by

$$\begin{aligned} &\varepsilon_\theta = (u + v_{,\theta})/r, \quad \gamma_{zr} = w_{,r}, \quad E_\theta = -\phi_{,\theta}/r \\ &\varepsilon_z = 0, \quad \gamma_{r\theta} = (u_{,\theta} - v)/r + v_{,r}, \quad E_z = 0 \\ &\varepsilon_r = u_{,r}, \quad \gamma_{\theta z} = w_{,\theta}/r, \quad E_r = -\phi_{,r} \end{aligned} \tag{1}$$

A subscript comma denotes differentiation with respect to a spatial coordinate. Using Eq. (1), the 3D constitutive equations of the piezoelectric medium with principal material axis 1 at angle $\beta$ to $\theta$-axis can

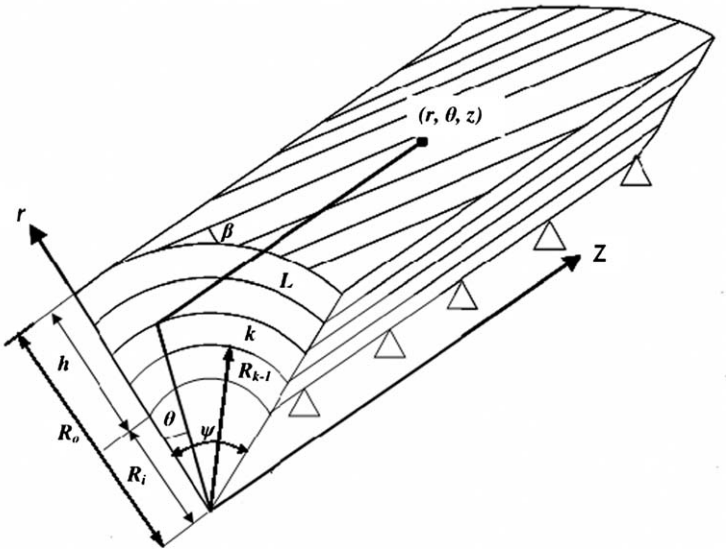


Fig. 1. Geometry of laminated hybrid cylindrical panel.

be expressed as

$$(u+v_{,\theta})/r = \bar{s}_{11}\sigma_\theta + \bar{s}_{12}\sigma_z + \bar{s}_{13}\sigma_r + \bar{s}_{16}\tau_{\theta z} - \bar{d}_{31}\phi_{,r} \tag{2}$$

$$0 = \bar{s}_{12}\sigma_\theta + \bar{s}_{22}\sigma_z + \bar{s}_{23}\sigma_r + \bar{s}_{26}\tau_{\theta z} - \bar{d}_{32}\phi_{,r} \tag{3}$$

$$u_{,r} = \bar{s}_{13}\sigma_\theta + \bar{s}_{23}\sigma_z + \bar{s}_{33}\sigma_r + \bar{s}_{36}\tau_{\theta z} - \bar{d}_{33}\phi_{,r} \tag{4}$$

$$w_{,r} = \bar{s}_{44}\tau_{zr} + \bar{s}_{45}\tau_{r\theta} - \bar{d}_{14}\phi_{,\theta}/r \tag{5}$$

$$(u_{,\theta}-v)/r + v_{,r} = \bar{s}_{45}\tau_{zr} + \bar{s}_{55}\tau_{r\theta} - \bar{d}_{15}\phi_{,\theta}/r \tag{6}$$

$$w_{,\theta}/r = \bar{s}_{16}\sigma_\theta + \bar{s}_{26}\sigma_z + \bar{s}_{36}\sigma_r + \bar{s}_{66}\tau_{\theta z} - \bar{d}_{36}\phi_{,r} \tag{7}$$

$$D_\theta = \bar{d}_{14}\tau_{zr} + \bar{d}_{15}\tau_{r\theta} - \bar{\varepsilon}_{11}\phi_{,\theta}/r \tag{8}$$

$$D_z = \bar{d}_{24}\tau_{zr} + \bar{d}_{25}\tau_{r\theta} - \bar{\varepsilon}_{12}\phi_{,\theta}/r \tag{9}$$

$$D_r = \bar{d}_{31}\sigma_\theta + \bar{d}_{32}\sigma_z + \bar{d}_{33}\sigma_r + \bar{d}_{36}\tau_{\theta z} - \bar{\varepsilon}_{33}\phi_{,r} \tag{10}$$

where $\bar{s}_{ij}$, $\bar{d}_{ij}$ and $\bar{\varepsilon}_{ij}$ are the elastic compliances, piezoelectric strain coefficients and the dielectric constants, transformed into the structural coordinate system $\theta, z, r$. The equations of momentum and charge balance, without body force and charge source, are

$$\tau_{r\theta,r} + \sigma_{\theta,\theta}/r + 2\tau_{r\theta}/r = \rho\ddot{v} \tag{11}$$

$$\tau_{zr,r} + \tau_{\theta z,\theta}/r + \tau_{zr}/r = \rho\ddot{w} \tag{12}$$

$$\sigma_{r,r} + \tau_{r\theta,\theta}/r + (\sigma_r - \sigma_\theta)/r = \rho\ddot{u} \tag{13}$$

$$D_{r,r} + D_r/r + D_{\theta,\theta}/r = 0 \tag{14}$$

where an over-dot $(\dot{})$ denotes differentiation with respect to time $t$.

## 3. Boundary and interface conditions

Dimensionless circumferential coordinate $\xi$ and local thickness coordinate $\zeta^k$ for the $k$th layer are introduced as

$$\xi = \theta/\psi, \quad \zeta^{(k)} = (r - R_1^{(k)})/t^{(k)} \quad \text{with } R_1^{(k)} = R - h/2 + \sum_{i=1}^{k-1} t^{(i)} \tag{15}$$

The coordinates $\xi$ and $\zeta^{(k)}$ take values 0, 1 at $\theta = 0, \psi$ and $r = R_1^{(k)}, R_1^{(k)} + t^{(k)}$, respectively. Let the prescribed pressure and the electric potential $\phi$ or the electric displacement $D_r$ at the inner and outer surfaces of the panel be $p_1(\xi,t), \phi_1(\xi,t)$ or $D_1(\xi,t)$ and $p_2(\xi,t), \phi_2(\xi,t)$ or $D_2(\xi,t)$, respectively. A distributed viscous force is also considered to act on the outer surface of the panel with the distributed damping coefficient $c_d$ per unit area per unit radial velocity ($\dot{u}$). For actuation of embedded or surface bonded piezoelectric layers, let the number of interfaces where the potential is prescribed be $L_a$ with the $q$th prescribed potential being $\Phi_q(\xi,t)$ for the interface $n_q$. Thus the boundary conditions are

$$\text{at } \xi = 0, 1 : u = 0, \quad \sigma_\theta = 0, \quad \tau_{\theta z} = 0, \quad \phi = 0 \tag{16}$$

$$\text{at } r = R_i : \sigma_r = -p_1, \quad \tau_{r\theta} = 0, \quad \tau_{zr} = 0, \quad \phi = \phi_1 \quad \text{or } D_r = D_1 \tag{17}$$

$$\text{at } r = R_o : \sigma_r = -p_2 - c_d\dot{u}(\xi, R_0, t), \quad \tau_{r\theta} = 0, \quad \tau_{zr} = 0 \quad \phi = \phi_2 \quad \text{or } D_r = D_2 \tag{18}$$

The case of known prescribed electric potential $\phi = \phi_i$ at a surface corresponds to the closed circuit electric boundary condition and the case of known electric charge density, $D_r = D_i$, corresponds to the open circuit (OC) condition. The conditions of continuity at the interface between the perfectly bonded adjacent layers are

$$[(u, v, w, \sigma_r, \tau_{zr}, \tau_{r\theta}, \phi, D_r)|_{\zeta=1}]^{(k)} = [(u, v, w, \sigma_r, \tau_{zr}, \tau_{r\theta}, \phi, D_r)|_{\zeta=0}]^{(k+1)} \tag{19}$$

for $k = 1,\ 2, \ldots, L-1$, except for $D_r$ for the interfaces at $k = n_q$, $q = 1, \ldots, L_a$, where the electric potential is prescribed. For such surfaces, the continuity condition for $D_r$ is to replaced by the following conditions:

$$[\phi|_{\zeta=1}]^{(n_q)} = \Phi_q(\xi, t) \quad \text{for } q = 1, \ldots, L_a \tag{20}$$

## 4. General solution

The steady-state solution is presented for forced vibration under harmonic electromechanical load of forcing frequency $\omega$. The electromechanical loads are of separable form $g(\xi)\cos\omega t = \mathrm{Re}[g(\xi)\mathrm{e}^{\mathrm{i}\omega t}]$ as

$$\{p^i, \phi_i, D_i, \Phi_q\}(\xi, t) = \mathrm{Re}[\{p^i, \phi_i, D_i, \Phi_q\}(\xi)\mathrm{e}^{\mathrm{i}\omega t}] \tag{21}$$

where Re(...) denotes the real part of the complex number (...). Let all the entities be expressed as $\mathrm{Re}[f(\xi)\mathrm{e}^{\mathrm{i}\omega t}]$, where $f(\xi)$ may be complex. The solution of the governing field equations for the $k$th layer, satisfying the boundary conditions (16), is expanded in the following Fourier series:

$$\begin{aligned}(u, \sigma_r, \sigma_\theta, \sigma_z, \tau_{\theta z}, \phi, D_r) &= \sum_{n=1}^{\infty} \mathrm{Re}[(u, \sigma_r, \sigma_\theta, \sigma_z, \tau_{\theta z}, \phi, D_r)_n \mathrm{e}^{\mathrm{i}\omega t}] \sin n\pi\xi \\ (v, w, \tau_{zr}, \tau_{r\theta}, D_\theta, D_z) &= \sum_{n=1}^{\infty} \mathrm{Re}[(v, w, \tau_{zr}, \tau_{r\theta}, D_\theta, D_z)_n \mathrm{e}^{\mathrm{i}\omega t}] \cos n\pi\xi\end{aligned} \tag{22}$$

The electromechanical loading functions are similarly expanded as

$$(p_i, \phi_i, D_i, \Phi_q) = \sum_{n=1}^{\infty} \mathrm{Re}[(p_i, \phi_i, D_i, \Phi_i)_n \mathrm{e}^{\mathrm{i}\omega t}] \sin n\pi\xi \tag{23}$$

On substitution of expansions (22), the governing partial differential equations (2)–(14) reduce to the following algebraic and ODEs:

$$(u_n - \bar{n}v_n)/r = \bar{s}_{11}\sigma_{\theta_n} + \bar{s}_{12}\sigma_{z_n} + \bar{s}_{13}\sigma_{r_n} + \bar{s}_{16}\tau_{\theta z_n} - \bar{d}_{31}\phi_{n,r} \tag{24}$$

$$0 = \bar{s}_{12}\sigma_{\theta_n} + \bar{s}_{22}\sigma_{z_n} + \bar{s}_{23}\sigma_{r_n} + \bar{s}_{26}\tau_{\theta z_n} - \bar{d}_{32}\phi_{n,r} \tag{25}$$

$$u_{n,r} = \bar{s}_{13}\sigma_{\theta_n} + \bar{s}_{23}\sigma_{z_n} + \bar{s}_{33}\sigma_{r_n} + \bar{s}_{36}\tau_{\theta z_n} - \bar{d}_{33}\phi_{n,r} \tag{26}$$

$$w_{n,r} = \bar{s}_{44}\tau_{zr_n} + \bar{s}_{45}\tau_{r\theta_n} - \bar{n}\bar{d}_{14}\phi_n/r \tag{27}$$

$$(\bar{n}u_n - v_n)/r + v_{n,r} = \bar{s}_{45}\tau_{zr_n} + \bar{s}_{55}\tau_{r\theta_n} - \bar{n}\bar{d}_{15}\phi_n/r \tag{28}$$

$$-\bar{n}w_n/r = \bar{s}_{16}\sigma_{\theta_n} + \bar{s}_{26}\sigma_{z_n} + \bar{s}_{36}\sigma_{r_n} + \bar{s}_{66}\tau_{\theta z_n} - \bar{d}_{36}\phi_{n,r} \tag{29}$$

$$D_{\theta_n} = \bar{d}_{14}\tau_{zr_n} + \bar{d}_{15}\tau_{r\theta_n} - \bar{n}\bar{\varepsilon}_{11}\phi_n/r \tag{30}$$

$$D_{z_n} = \bar{d}_{24}\tau_{zr_n} + \bar{d}_{25}\tau_{r\theta_n} - \bar{n}\bar{\varepsilon}_{12}\phi_n/r \tag{31}$$

$$D_{r_n} = \bar{d}_{31}\sigma_{\theta_n} + \bar{d}_{32}\sigma_{z_n} + \bar{d}_{33}\sigma_{r_n} + \bar{d}_{36}\tau_{\theta z_n} - \bar{\varepsilon}_{33}\phi_{n,r} \tag{32}$$

$$(\sigma_{rn})_{,r} + (-\bar{n}\tau_{r\theta_n} + \sigma_{r_n} - \sigma_{\theta_n})/r = -\rho\omega^2 u_n \tag{33}$$

$$(\tau_{r\theta_n})_{,r} + (\bar{n}\sigma_{\theta_n} + 2\tau_{r\theta_n})/r = -\rho\omega^2 v_n \tag{34}$$

$$(\tau_{zr_n})_{,r} + (\bar{n}\tau_{\theta z_n} + \tau_{zr_n})/r = -\rho\omega^2 w_n \tag{35}$$

$$(D_{r_n})_{,r} + D_{r_n}/r - \bar{n}D_{\theta_n}/r = 0 \tag{36}$$

where $\bar{n} = n\pi/\psi$. These 13 governing equations are transformed into eight first-order ODEs in terms of eight independent variables in $X$:

$$X = [v_n \;\; w_n \;\; u_n \;\; \sigma_{r_n} \;\; \tau_{zr_n} \;\; \tau_{r\theta_n} \;\; \phi_n \;\; D_{r_n}]^{\mathrm{T}} \tag{37}$$

which appear in the boundary and interface conditions given by Eqs. (16)–(20) and five algebraic equations for the remaining dependent variables $\sigma_{\theta_n}, \sigma_{z_n}, \tau_{\theta z_n}, D_{\theta_n}, D_{z_n}$. Substituting $\phi_{n,r}$ from Eq. (32) into Eqs. (24), (25), (29) and (26) yields

$$\frac{1}{r}\begin{bmatrix} u_n - \bar{n}v_n \\ 0 \\ -\bar{n}w_n \\ ru_{n,r} \end{bmatrix} = \begin{bmatrix} \bar{s}'_{11} & \bar{s}'_{12} & \bar{s}'_{16} \\ \bar{s}'_{12} & \bar{s}'_{22} & \bar{s}'_{26} \\ \bar{s}'_{16} & \bar{s}'_{26} & \bar{s}'_{66} \\ \bar{s}'_{13} & \bar{s}'_{23} & \bar{s}'_{36} \end{bmatrix} \begin{bmatrix} \sigma_{\theta_n} \\ \sigma_{z_n} \\ \tau_{\theta z_n} \end{bmatrix} + \begin{bmatrix} \bar{s}'_{13} \\ \bar{s}'_{23} \\ \bar{s}'_{36} \\ \bar{s}'_{33} \end{bmatrix} \sigma_{r_n} + \begin{bmatrix} \bar{d}'_{31} \\ \bar{d}'_{32} \\ \bar{d}'_{36} \\ \bar{d}'_{33} \end{bmatrix} D_{r_n} \tag{38}$$

where

$$\bar{d}'_{ij} = \bar{d}_{ij}/\bar{\varepsilon}_{33}, \quad \bar{s}'_{ij} = \bar{s}_{ij} - \bar{d}_{3i}\bar{d}'_{3j} \tag{39}$$

Inverting equations $(38)_{1,2,3}$, the algebraic expressions are obtained for $\sigma_{\theta_n}, \sigma_{z_n}, \tau_{\theta z_n}$ in terms of the elements of $X$:

$$\begin{aligned} \sigma_{\theta_n} &= p_{11}(\bar{n}v_n - u_n)/r + \bar{n}p_{12}w_n/r + p_{14}\sigma_{r_n} + p_{18}D_{r_n} \\ \sigma_{z_n} &= p_{21}(\bar{n}v_n - u_n)/r + \bar{n}p_{22}w_n/r + p_{24}\sigma_{r_n} + p_{28}D_{r_n} \\ \tau_{\theta z_n} &= p_{61}(\bar{n}v_n - u_n)/r + \bar{n}p_{62}w_n/r + p_{64}\sigma_{r_n} + p_{68}D_{r_n} \end{aligned} \tag{40}$$

with

$$\begin{aligned} p_{i1} &= -\hat{s}_{i1}, \quad p_{i4} = -(\hat{s}_{i1}\bar{s}'_{13} + \hat{s}_{i2}\bar{s}'_{23} + \hat{s}_{i6}\bar{s}'_{36}) \\ p_{i2} &= -\hat{s}_{i6}, \quad p_{i8} = -(\hat{s}_{i1}\bar{d}'_{31} + \hat{s}_{i2}\bar{d}'_{32} + \hat{s}_{i6}\bar{d}'_{36}) \\ \begin{bmatrix} \hat{s}_{11} & \hat{s}_{12} & \hat{s}_{16} \\ \hat{s}_{21} & \hat{s}_{22} & \hat{s}_{26} \\ \hat{s}_{61} & \hat{s}_{62} & \hat{s}_{66} \end{bmatrix} &= \begin{bmatrix} \bar{s}'_{11} & \bar{s}'_{12} & \bar{s}'_{16} \\ \bar{s}'_{12} & \bar{s}'_{22} & \bar{s}'_{26} \\ \bar{s}'_{16} & \bar{s}'_{26} & \bar{s}'_{66} \end{bmatrix}^{-1} \end{aligned} \tag{41}$$

for $i = 1, 2, 6$. Eqs. (30) and (31) are the algebraic equations for $D_{\theta_n}, D_{z_n}$ in terms of the elements of $X$. Substitution of $\sigma_{\theta_n}, \sigma_{z_n}, \tau_{\theta z_n}$ from Eq. (40), $D_{\theta_n}$ from Eq. (30) and $\phi_{n,r}$ from Eq. (32) into Eqs. $(38)_4$, (27), (28), (32)–(36) yields the following first-order homogeneous ODEs with variable coefficients which can be expressed in matrix form as

$$X_{,r} = (A_0 + A_1/r + A_2/r^2)X \tag{42}$$

The non-zero elements of matrices $A_0, A_1, A_2$ are

$$\begin{aligned} &A_0(1,5) = \bar{s}_{45}, \quad A_1(3,1) = \bar{n}p^s_1, \quad A_2(4,1) = \bar{n}p_{11} \\ &A_0(1,6) = \bar{s}_{55}, \quad A_1(3,2) = \bar{n}p^s_2, \quad A_2(4,2) = \bar{n}p_{12} \\ &A_0(2,5) = \bar{s}_{44}, \quad A_1(3,3) = -p^s_1, \quad A_2(4,3) = -p_{11} \\ &A_0(2,6) = \bar{s}_{45}, \quad A_1(4,4) = p_{14} - 1, \quad A_2(5,1) = -\bar{n}^2 p_{61} \\ &A_0(3,4) = p^s_4 + \bar{s}'_{33}, \quad A_1(4,6) = \bar{n}, \quad A_2(5,2) = -\bar{n}^2 p_{62} \\ &A_0(3,8) = p^s_8 + \bar{d}'_{33}, \quad A_1(4,8) = p_{18}, \quad A_2(5,3) = \bar{n}p_{61} \\ &A_0(4,3) = -\rho\omega^2, \quad A_1(5,4) = -\bar{n}p_{64}, \quad A_2(6,1) = -\bar{n}^2 p_{11} \end{aligned} \tag{43}$$

$$
\begin{aligned}
&A_0(5,2) = -\rho\omega^2, \quad A_1(5,5) = -1, \quad A_2(6,2) = -\bar{n}^2 p_{12}\\
&A_0(6,1) = -\rho\omega^2, \quad A_1(5,8) = -\bar{n}p_{68}, \quad A_2(6,3) = \bar{n}p_{11}\\
&A_0(7,4) = p_4^d + \bar{d}'_{33} \quad A_1(6,4) = -\bar{n}p_{14}, \quad A_1(7,3) = -p_1^d\\
&A_0(7,8) = p_8^d - 1/\bar{\varepsilon}_{33} \quad A_1(6,6) = -2, \quad A_1(8,5) = \bar{n}\bar{d}_{14}\\
&A_1(1,1) = 1, \quad A_1(6,8) = -\bar{n}p_{18}, \quad A_1(8,6) = \bar{n}\bar{d}_{15}\\
&A_1(1,3) = -\bar{n}, \quad A_1(7,1) = \bar{n}p_1^d, \quad A_2(8,7) = -\bar{n}^2\bar{\varepsilon}_{11}\\
&A_1(1,7) = -\bar{n}\bar{d}_{15}, \quad A_1(7,2) = \bar{n}p_2^d, \quad A_1(8,8) = -1\\
&A_1(2,7) = -\bar{n}\bar{d}_{14}
\end{aligned}
\tag{44}
$$

where

$$
\begin{aligned}
p_i^s &= \bar{s}'_{13}p_{1i} + \bar{s}'_{23}p_{2i} + \bar{s}'_{36}p_{6i}\\
p_i^d &= \bar{d}'_{31}p_{1i} + \bar{d}'_{32}p_{2i} + \bar{d}'_{36}p_{6i}
\end{aligned}
\tag{45}
$$

The general solution of Eq. (42) is obtained using modified Frobenius method [17,18] wherein the solution is expanded in terms of the product of an exponential function and a power series in the dimensionless thickness coordinate $\zeta$ ($0 \leqslant \zeta \leqslant 1$):

$$
X(\zeta) = \mathrm{e}^{\lambda\zeta}\sum_{i=0}^{\infty} Z_i\zeta^i \tag{46}
$$

$$
\Rightarrow \quad X_{,\zeta} = \mathrm{e}^{\lambda\zeta}\sum_{i=0}^{\infty}[\lambda Z_i + (i+1)Z_{i+1}]\zeta^i \tag{47}
$$

This method differs from the conventional Frobenius method [25] in which the solution is assumed as a product of the radial coordinate raised to a power ($r^\lambda$) and a power series in that coordinate. It can be readily seen that in the modified method, one term solution in the power series ensures the exact solution of Eq. (42) for the case of constant coefficients with values corresponding to $\zeta = 0$ (i.e. $r = R_1^{(k)}$). This is, however, not the case for the conventional Frobenius and power series methods. Consequently, this modified method yields much faster convergence compared to the latter methods. Also, the modified method has not led to multiple roots for any of the numerical studies conducted earlier [17–19] for shells. Using $(15)_2$, the governing equation (42) can be expressed as

$$
\begin{aligned}
&(s+\zeta)^2 X_{,\zeta} = [R_1A_0(s+\zeta)^2/s + A_1(s+\zeta) + A_2 s/R_1]X\\
&\Rightarrow (s^2 + 2s\xi + \xi^2)X_{,\zeta} = [s^2A + (2R_1A_0 + A_1)\zeta + A_0 t\zeta^2]X
\end{aligned}
\tag{48}
$$

$$
A = [A_0R_1 + A_1 + A_2/R_1]/s \tag{49}
$$

where $s = R_1/t$. Substituting the solution from Eqs. (46) and (47) into Eq. (48) yields

$$
\begin{aligned}
&\sum_{i=0}^{\infty}[\{\lambda Z_i + (i+1)Z_{i+1}\}(s^2 + 2s\zeta + \zeta^2) - \{s^2A + (2R_1A_0 + A_1)\zeta + A_0t\zeta^2\}Z_i]\zeta^i = 0\\
&\Rightarrow \sum_{i=0}^{\infty}[s^2(i+1)Z_{i+1} - s^2\{A - (\lambda + 2i/s)I\}Z_i\\
&\quad - \{2R_1A_0 + A_1 - (2\lambda s + i - 1)I\}Z_{i-1} - (tA_0 - \lambda I)Z_{i-2}]\zeta^i = 0
\end{aligned}
\tag{a}
$$

where a term $Z_j$ is included only if $j \geqslant 0$. In Eq. (a), setting the coefficients of $\zeta^0$ and of $\xi^i$ as zero for $i \geqslant 1$ yields

$$
s^2Z_1 - s^2(A - \lambda I)Z_0 = 0 \tag{b}
$$

and a recursive relation for $Z_i$:

$$
Z_{i+1} = [d_0(\lambda, i)Z_i + d_1(\lambda, i)Z_{i-1} + d_2(\lambda)Z_{i-2}]/(i+1), \quad i \geqslant 1 \tag{c}
$$

where

$$d_0(\lambda,i) = A - (\lambda + 2i/s)I$$
$$d_1(\lambda,i) = [2R_1A_0 + A_1 - (2\lambda s + i - 1)I]/s^2$$
$$d_2(\lambda) = (tA_0 - \lambda I)/s^2 \tag{50}$$

The indicial equation for $\lambda$ is obtained from Eq. (b) by choosing $Z_1 = 0$, which yields

$$AZ_0 = \lambda Z_0 \tag{51}$$

Hence the exponent $\lambda$ and $Z_0$ are the eigenvalue and eigenvector pair of $8 \times 8$ real matrix $A$. Since $A$ has eight eigenpairs $(\lambda_j, Z_0^j)$, $j = 1,\ldots,8$; $X$ is the sum of eight solutions of the form (46) with the exponential factor $e^{\lambda_j\zeta}$ and coefficients $Z_i^j$ for the power series for the $j$th solution. $Z_0^j$ is the normalized eigenvector and $Z_1^j = 0$. The other coefficients of the series are obtained using Eq. (c) for $\lambda = \lambda_j$:

$$Z_{i+1}^j = [d_0(\lambda_j,i)Z_i^j + d_1(\lambda_j,i)Z_{i-1}^j + d_2(\lambda_j)Z_{i-2}^j]/(i+1), \quad i \geqslant 1 \tag{52}$$

The eigenvalues of $A$ are either real or occur in complex conjugate pairs. The solution for pair of eigenvalues $\lambda_1, \lambda_2 = \alpha \pm i\beta$ with complex eigenvector $Z_0^1$ corresponding to $\lambda_1$ can be expressed in terms of two real constants $C_1$ and $C_2$ as

$$X(\zeta) = F_1(\zeta)C_1 + F_2(\zeta)C_2 \tag{53}$$

$$F_1(\zeta) = e^{\alpha\zeta}\left[\cos\beta\zeta \sum_{i=0}^{\infty} \mathrm{Re}(Z_i^1)\zeta^i - \sin\beta\zeta \sum_{i=0}^{\infty} \mathrm{Im}(Z_i^1)\zeta^i\right] \tag{54}$$

$$F_2(\zeta) = e^{\alpha\zeta}\left[\sin\beta\zeta \sum_{i=0}^{\infty} \mathrm{Re}(Z_i^1)\zeta^i + \cos\beta\zeta \sum_{i=0}^{\infty} \mathrm{Im}(Z_i^1)\zeta^i\right] \tag{55}$$

Re and Im indicate real and imaginary parts of a complex number. The solution for distinct real eigenvalue, say $\lambda_3 = p$ with eigenvector $Z_0^3$, in terms of real constant $C_3$, is

$$X_{(\zeta)} = F_3(\zeta)C_3, \quad F_3(\zeta) = e^{p\zeta}\left[\sum_{i=0}^{\infty} Z_i^3\zeta^i\right] \tag{56}$$

The general solution $X(\zeta)$ can be expressed in terms of real constants $C_j$ as

$$X(\zeta) = \sum_{j=1}^{8} F_j(\zeta)C_j = F(\zeta)C \tag{57}$$

where

$$F(\zeta) = [F_1(\zeta)\ \ F_2(\zeta)\ \ F_3(\zeta)\ \ F_4(\zeta)\ \ F_5(\zeta)\ \ F_6(\zeta)\ \ F_7(\zeta)\ \ F_8(\zeta)]$$
$$C = [C_1\ \ C_2\ \ C_3\ \ C_4\ \ C_5\ \ C_6\ \ C_7\ \ C_8]^{\mathrm{T}} \tag{58}$$

The functional form of $F_j(\zeta)$ is given by Eqs. (54), (55) or $(56)_2$ as per the nature of $\lambda_j$. The infinite power series in $F_j(\zeta)$ are truncated to finite number of terms such that the contribution of the first neglected term is less than a stipulated small number $\eta$ $(= 10^{-10})$. For the $k$th layer, the values $X_k^-$ of $X$ at the top $(\zeta = 1)$ can be reduced to the value $X_{k-1}^+$ of $X$ at the bottom $(\zeta = 0)$ as follows:

$$X(0) = F(0)C, \quad \Rightarrow \quad C = [F(0)]^{-1}X(0)$$
$$X(1) = F(1)C = F(1)[F(0)]^{-1}X(0)$$
$$\Rightarrow \quad X_k^- = T_kX_{k-1}^+ \quad \text{with } T_k = F(1)[F(0)]^{-1} \tag{59}$$

$T_k$ is called the transfer matrix for the $k$th layer. Following the transfer matrix method detailed in Ref. [7], the values $X_L$ of $X$ at the top of the laminate are related to the values $X_0$ of $X$ at the bottom of the laminate by using the continuity conditions in Eqs. (19) and (20). Out of the 16 variables in $X_L$ and $X_0$, eight are eliminated from the eight boundary conditions in Eqs. (17) and (18), yielding eight algebraic equation for the

remaining eight variables. The undamped natural frequencies $\omega = \omega_n$ are obtained using the procedure of Kapuria and Achary [7].

## 5. Numerical results

### 5.1. Validation

The results obtained from the present formulation are validated by comparing with results for natural frequencies of an elastic cylindrical panel presented by Chen and Lee [21] using the layerwise method. A five layered cylindrical panel with lay-up $[-15^\circ/60^\circ/90^\circ/75^\circ/-45^\circ]$ of stacking sequence from bottom to top, having same thickness for all plies and same density ratio is considered for validation. The material properties are considered as $Y_L/Y_T = 25$, $G_{LT}/Y_T = 0.5$, $G_{TT}/Y_T = .2$, $\mu_{LT} = \mu_{TT} = 0.25$, where $Y$ is Young's modulus, $G$ the shear modulus, $\mu$ Poisson's ratio and subscripts $L$ and $T$ indicate, respectively, directions parallel and perpendicular to the fibers. The span angle of the panel is taken to be $\psi = \pi/3$. The lowest 10 dimensionless frequencies ($\omega^* = \omega R_i\sqrt{\rho/Y_T}$) for two lower modes $n = 1$ and 2 are compared in Table 1. It is observed that the present results match exactly with those of Ref. [21].

### 5.2. Free vibration

Benchmark results are presented for piezoelectric hybrid shell panels of four configurations (a), (b), (c) and (d) as shown in Fig. 2. Panel (a) is a single layer piezoelectric panel of made of PZT-5A. Panel (b) is a hybrid angle-ply test panel which is highly inhomogeneous in material properties. Panels (c) and (d) are hybrid angle-ply composite and sandwich panels, respectively. The properties [10] of materials of the laminas are $[(Y_1, Y_2, Y_3, G_{12}, G_{23}, G_{31}), v_{12}, v_{13}, v_{23}] =$

Material 1: $[(6.9, 6.9, 6.9, 2.76, 2.76, 2.76)\,\text{GPa},\ 0.25, 0.25, 0.25]$
Material 2: $[(224.25, 6.9, 6.9, 56.58, 1.38, 56.58)\,\text{GPa},\ 0.25, 0.25, 0.25]$

Table 1
Comparison of frequency parameters $\omega^*$ of five layered simply supported elastic angle-ply composite cylindrical panel in cylindrical bending.

| $n$ | Order | $S = 4$ | | $S = 20$ | |
|---|---|---|---|---|---|
| | | Chen and Lee [21] | Present | Chen and Lee [21] | Present |
| 1 | 1 | 0.800913 | 0.8009137 | 0.297289 | 0.2972891 |
| | 2 | 3.68538 | 3.685381 | 4.57717 | 4.577165 |
| | 3 | 5.45687 | 5.456873 | 8.14466 | 8.144664 |
| | 4 | 7.93727 | 7.937278 | 30.1375 | 30.13755 |
| | 5 | 9.73254 | 9.732535 | 39.6732 | 39.67323 |
| | 6 | 11.2964 | 11.29636 | 60.5671 | 60.56711 |
| | 7 | 13.1383 | 13.13831 | 63.6877 | 63.68769 |
| | 8 | 14.3726 | 14.37256 | 70.6553 | 70.65526 |
| | 9 | 17.6276 | 17.62756 | 91.8882 | 91.88824 |
| | 10 | 19.9383 | 19.93832 | 105.671 | 105.6706 |
| 2 | 1 | 2.17166 | 2.171660 | 1.20765 | 1.207655 |
| | 2 | 6.46837 | 6.468361 | 8.92641 | 8.926406 |
| | 3 | 7.89499 | 7.894998 | 15.0668 | 15.06679 |
| | 4 | 9.75943 | 9.759445 | 34.5660 | 34.56596 |
| | 5 | 11.7353 | 11.73526 | 40.6152 | 40.61517 |
| | 6 | 13.4791 | 13.47908 | 61.3742 | 61.37415 |
| | 7 | 14.6435 | 14.64350 | 64.5697 | 64.56972 |
| | 8 | 18.6976 | 18.69753 | 70.9909 | 70.99092 |
| | 9 | 19.7625 | 19.76246 | 92.4875 | 92.48745 |
| | 10 | 22.9928 | 22.99279 | 106.133 | 106.1325 |

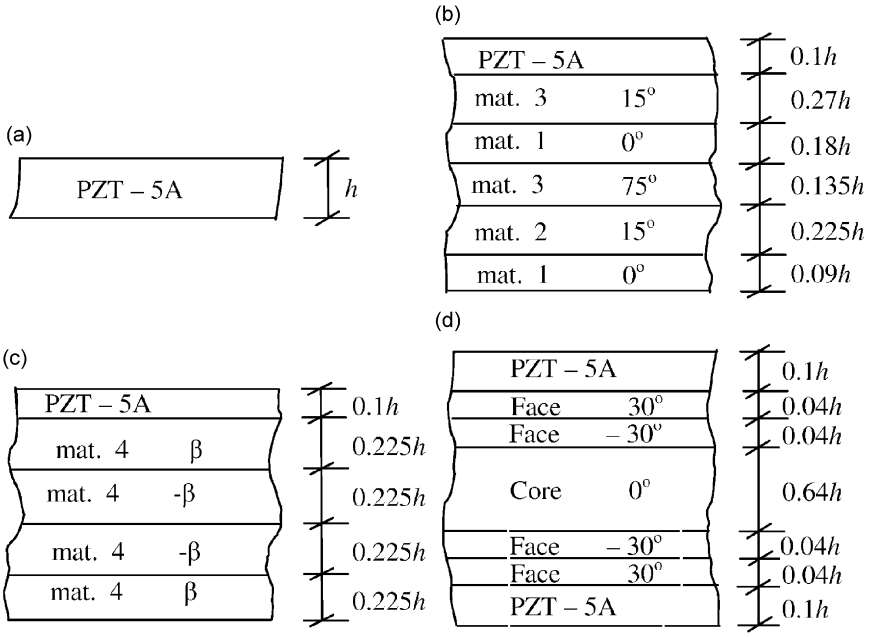


Fig. 2. Configurations of hybrid cylindrical panels (a), (b), (c) and (d).

Material 3: [(172.5, 6.9, 6.9, 3.45, 1.38, 3.45) GPa, 0.25, 0.25, 0.25]
Material 4: [(181.0, 10.3, 10.3, 7.17, 2.87, 7.17) GPa, 0.28, 0.28, 0.33]
Face: [(131.1, 6.9, 6.9, 3.088, 2.3322, 3.588) GPa, 0.32, 0.32, 0.49]
Core: [(0.2208, 0.2001, 2760, 16.56, 455.4, 545.1) MPa, $0.99, 3\times10^{-5}, 3\times10^{-5}$]
PZT-5A: [(61.0, 61.0, 53.2, 22.6, 21.1, 21.1) GPa, 0.35, 0.38, 0.38], and $[(d_{31}, d_{32}, d_{33}, d_{15}, d_{24}), (\eta_{11}, \eta_{22}, \eta_{33})] = [(-171, -171, 374, 584, 584)\times10^{-12}\ \mathrm{m\,V^{-1}}, (1.53, 1.53, 1.5)\times10^{-8}\ \mathrm{F\,m^{-1}}]$. The density of materials 1, 2, 3, 4 is 1578 $\mathrm{kg\,m^{-3}}$and of PZT-5A, face and core materials is 7600, 1000 and 70 $\mathrm{kg\,m^{-3}}$, respectively.

The interface between elastic substrate and piezoelectric layer is electrically grounded. The inner surfaces of panels (a) and (d) are at OC condition. In order to assess the effect of electric boundary conditions, both close circuit (CC) and OC conditions are considered for the outer surface of the panels.

The natural frequencies $\omega_n$ and the modal displacements are non-dimensionalized as

$$\bar{\omega}_n = \omega_n R S_1 (\rho_0/Y_0)^{1/2}, \quad (\bar{u}, \bar{v}, \bar{w}) = (u, v, w)/\max(u, v, w)$$

where $Y_0 = 61.9$ GPa for panel (a), $Y_0 = 6.9$ GPa for panels (b), (d), and $Y_0 = 10.3$ GPa for panel (c); $\rho_0 = 7600\ \mathrm{kg\,m^{-3}}$ for panel (a), 1578 $\mathrm{kg\,m^{-3}}$ for panels (b), (c) and 1000 $\mathrm{kg\,m^{-3}}$ for panel (d). The expression $\max(u, v, w)$ denotes the largest value of $u, v$ and $w$ through the thickness for a given vibration mode, and $S_1 = S, 1, 1/S$ for thickness mode 1, modes 2, 3 and modes 4, 5, 6, 7, respectively. $S$ is the mean radius to thickness ratio ($R/h$). The dimensionless undamped natural frequencies of the simply supported cylindrical panels of all four configurations (a), (b), (c) and (d) with span angle $\psi = 60^\circ$ are presented in Table 2 under OC condition for three values of $S = 5, 10, 20$. For panel (c), the ply angle $\beta$ is taken as 30°. The frequencies are listed for lowest seven thickness modes for the spatial mode $n = 1$ and only the flexural mode 1 for the spatial modes $n = 2$ and 3. Typical through-the-thickness distributions of modal displacements $\bar{u}$, $\bar{v}$ and $\bar{w}$ are plotted in Fig. 3 for hybrid panel (d) under OC condition for the lowest seven thickness modes for spatial mode $n = 1$ and $S = 20$. The mode shapes indicate that the first mode is a bending mode and the second and third modes are extensional modes along axial and circumferential directions, respectively. The fourth and fifth modes correspond to thickness shear modes distinguished by antisymmetric inplane displacements and zero transverse displacement. The sixth mode corresponds to thickness stretching and the seventh one is a

Table 2
Natural frequencies $\bar{\omega}_n$ of hybrid cylindrical panels under open circuit condition (OC).

| $n$ | Mode | $\psi = 60^\circ$ | | | | | $\psi = 120^\circ$ |
|---|---|---|---|---|---|---|---|
| | | $S$ | Panel (a) | Panel (b) | Panel (c) | Panel (d) | Panel (d) |
| 1 | 1 | 5 | 2.4313 | 4.6473 | 4.3318 | 2.4555 | 0.50119 |
| | | 10 | 2.5210 | 6.3075 | 5.3447 | 3.6897 | 0.61580 |
| | | 20 | 2.5456 | 7.1479 | 5.7485 | 4.5097 | 0.66016 |
| | 2 | 5 | 3.6220 | 3.5165 | 4.2030 | 2.5294 | 1.2811 |
| | | 10 | 3.6709 | 3.9373 | 4.5811 | 2.5636 | 1.2833 |
| | | 20 | 3.6826 | 4.0608 | 4.6846 | 2.5655 | 1.2829 |
| | 3 | 5 | 11.354 | 8.3583 | 7.0492 | 3.5877 | 2.6982 |
| | | 10 | 21.649 | 9.7064 | 8.1351 | 4.9072 | 2.8107 |
| | | 20 | 42.760 | 10.153 | 8.4833 | 4.9536 | 2.8258 |
| | 4 | 5 | 3.5619 | 1.7263 | 1.7813 | 0.90641 | 0.55121 |
| | | 10 | 3.6318 | 1.3836 | 1.5217 | 0.54820 | 0.50063 |
| | | 20 | 3.6581 | 1.2992 | 1.4468 | 0.50024 | 0.48771 |
| | 5 | 5 | 4.2267 | 2.5495 | 2.5108 | 1.0745 | 0.72913 |
| | | 10 | 4.0926 | 1.9991 | 1.9941 | 0.71341 | 0.58267 |
| | | 20 | 4.0502 | 1.7363 | 1.8320 | 0.58057 | 0.54289 |
| | 6 | 5 | 5.6318 | 2.8180 | 2.8060 | 1.3084 | 1.2285 |
| | | 10 | 5.6201 | 2.6559 | 2.6794 | 1.1880 | 1.1861 |
| | | 20 | 5.6173 | 2.6442 | 2.6713 | 1.1776 | 1.1775 |
| | 7 | 5 | 8.1005 | 3.0168 | 3.4291 | 5.0420 | 5.0393 |
| | | 10 | 8.0771 | 2.7286 | 3.3107 | 5.0367 | 5.0360 |
| | | 20 | 8.0712 | 2.6937 | 3.2850 | 5.0354 | 5.0352 |
| 2 | 1 | 5 | 9.6614 | 13.352 | 13.228 | 6.5164 | 2.4555 |
| | | 10 | 10.992 | 21.278 | 19.729 | 11.180 | 3.6897 |
| | | 20 | 11.449 | 28.780 | 24.304 | 16.813 | 4.5097 |
| 3 | 1 | 5 | 19.016 | 22.822 | 22.422 | 10.911 | 4.4450 |
| | | 10 | 23.800 | 37.747 | 36.728 | 18.860 | 7.3823 |
| | | 20 | 25.890 | 57.011 | 50.638 | 31.260 | 10.173 |

higher-order thickness shear mode along circumferential direction. While the above thickness modes are found to hold well for hybrid shells of all lay-ups for $S \geqslant 10$, their order has been found to be different in some cases for $S = 5$.

Similar results for frequencies for CC condition at the outer surface are presented in Table 3. As expected, the natural frequencies for OC condition are higher than those for CC condition, which is due to increase in effective stiffness caused by direct piezoelectric effect in the former case. It is revealed that while the difference between the OC and the CC flexural frequencies decrease with the increase in $S$ for the single layer piezoelectric panel (a), it increases with $S$ for all hybrid panels (b), (c) and (d). Consistent with this, for higher flexural modes, this difference is smaller for piezoelectric panel (a) and larger for the hybrid panels. The natural frequencies for a deeper shell panel (d) with span angle $\psi = 120^\circ$ are also listed in Table 2. Being more flexible, its frequencies are lesser than those of the shell with $\psi = 60^\circ$, for thickness modes 1–5. Frequencies of thickness modes 6 and 7 are not much affected by the span angle. Fig. 4 depicts the effect of ply-angle on natural frequencies of the first three flexural modes of hybrid angle-ply composite panel (c) for $S = 5$ and 10. As expected, the natural frequencies decrease with the increase in ply-angle.

### 5.3. Forced vibration

The steady-state harmonic response is obtained for the following two load cases:

(1) Pressure $p_2 = -p_0 \sin(\pi\theta/\psi)$ on the outer surface with electric boundary condition (OC).
(2) Potential $\phi_2 = \phi_0 \sin(\pi\theta/\psi)$ applied to the outer surface with electric boundary condition (CC).

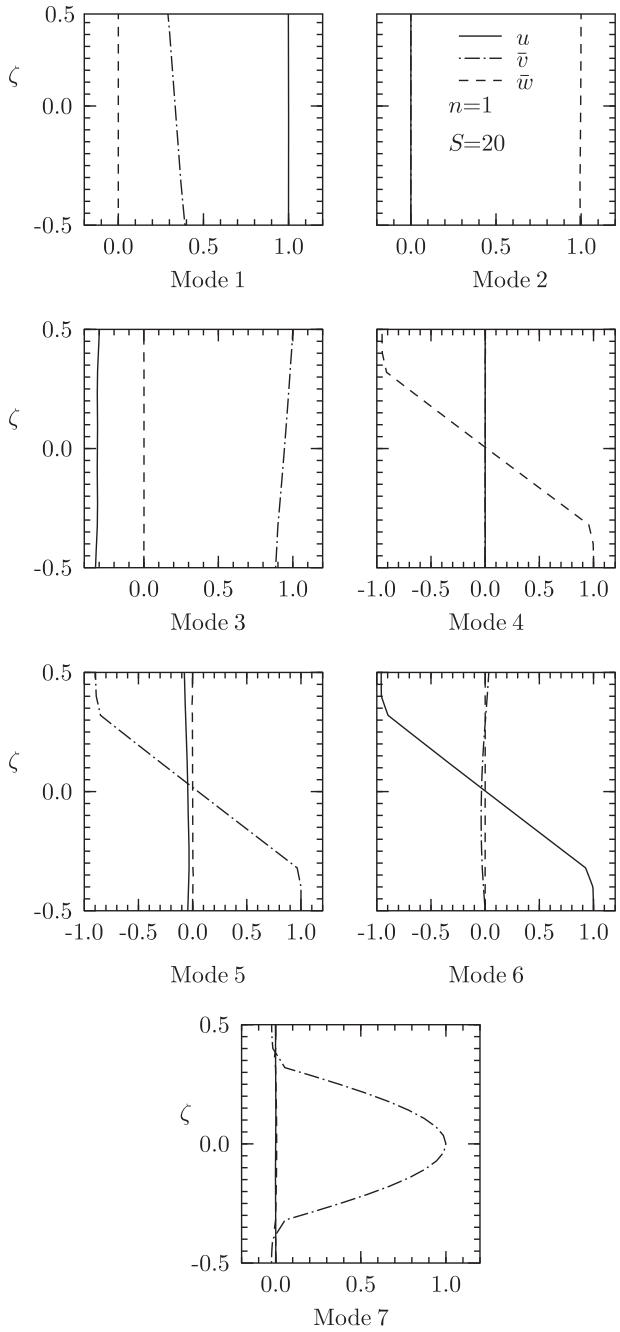


Fig. 3. Through-thickness distribution of $\bar{u}$, $\bar{v}$ and $\bar{w}$ for sandwich panel (d) for first seven thickness modes.

The results for these two load cases are non-dimensionalized as:

(1) $\bar{u} = 10uY_0/hS^4p_0,\ \bar{\sigma}_\theta = \sigma_\theta/S^2p_0, \quad \bar{\tau}_{r\theta} = \tau_{r\theta}/Sp_0,$
(2) $\bar{u} = u/S^2d_0\phi_0, \quad \bar{\sigma}_\theta = \sigma_\theta h/Y_0d_0\phi_0, \quad \bar{\tau}_{r\theta} = \tau_{r\theta}Sh/Y_0d_0\phi_0,$

where $d_0 = 374.0 \times 10^{-12}\,\mathrm{CN}^{-1}$ for all four panels and $Y_0$ is as given in Section 5.2. The damping parameter $\bar{c}$ is non-dimensionalized as $\bar{c} = c_dS/2\rho_0R\omega_1$.

Table 3
Natural frequencies $\bar{\omega}_n$ of hybrid cylindrical panels under close circuit condition (CC).

| $n$ | Mode | $S$ | Panel (a) | Panel (b) | Panel (c) | Panel (d) |
|---|---|---|---|---|---|---|
| 1 | 1 | 5 | 2.4183 | 4.6101 | 4.2785 | 2.4334 |
| | | 10 | 2.5171 | 6.2297 | 5.2605 | 3.6240 |
| | | 20 | 2.5446 | 7.0405 | 5.6483 | 4.3937 |
| | 2 | 5 | 3.5731 | 3.5025 | 4.2005 | 2.5294 |
| | | 10 | 3.6597 | 3.9275 | 4.5810 | 2.5636 |
| | | 20 | 3.6800 | 4.0530 | 4.6846 | 2.5655 |
| | 3 | 5 | 10.029 | 8.2986 | 6.9450 | 3.5876 |
| | | 10 | 18.771 | 9.6100 | 8.0588 | 4.7474 |
| | | 20 | 36.897 | 10.075 | 8.4192 | 4.8185 |
| | 4 | 5 | 3.5585 | 1.7124 | 1.7808 | 0.86802 |
| | | 10 | 3.6311 | 1.3834 | 1.5217 | 0.54820 |
| | | 20 | 3.6580 | 1.2990 | 1.4468 | 0.50024 |
| | 5 | 5 | 4.2101 | 2.5495 | 2.5102 | 1.0728 |
| | | 10 | 4.0877 | 1.9973 | 1.9925 | 0.70940 |
| | | 20 | 4.0489 | 1.7356 | 1.8314 | 0.57856 |
| | 6 | 5 | 5.5295 | 2.8166 | 2.8049 | 1.3044 |
| | | 10 | 5.5092 | 2.6559 | 2.6793 | 1.1876 |
| | | 20 | 5.5042 | 2.6442 | 2.6709 | 1.1775 |
| | 7 | 5 | 8.0949 | 3.0150 | 3.4290 | 5.0418 |
| | | 10 | 8.0754 | 2.7285 | 3.3107 | 5.0366 |
| | | 20 | 8.0708 | 2.6936 | 3.2850 | 5.0354 |
| 2 | 1 | 5 | 9.5517 | 13.283 | 13.107 | 6.4798 |
| | | 10 | 10.936 | 21.089 | 19.465 | 11.066 |
| | | 20 | 11.431 | 28.409 | 23.907 | 16.498 |
| 3 | 1 | 5 | 18.769 | 22.732 | 22.261 | 10.855 |
| | | 10 | 23.600 | 37.482 | 36.304 | 18.719 |
| | | 20 | 25.808 | 56.390 | 49.872 | 30.830 |

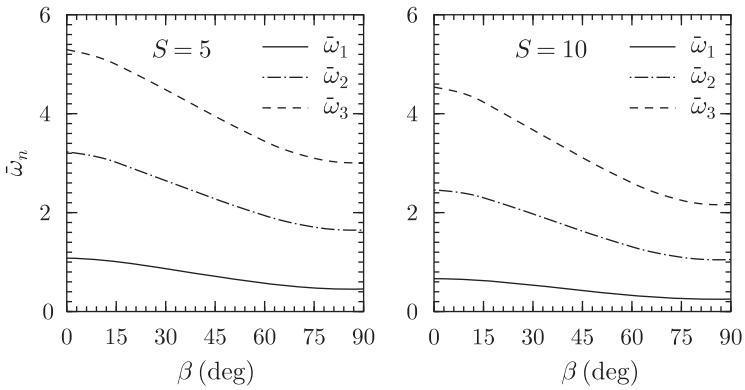


Fig. 4. Effect of ply-angle on flexural natural frequencies of hybrid angle-ply composite panel (c) under open circuit condition (OC).

The dimensionless values of amplitude of mid-surface deflection $\bar{u}_m$ at the center of the panels and its phase lag $\kappa^\circ$ for harmonic pressure load of case (1) are listed in Table 4 for two values of forcing frequency ratio $\omega/\omega_1 = 0.7, 1$ for $S = 5, 10$ and 20. Similar results for the potential load case (2) are presented in Table 5. Results are presented for both undamped and damped cases with $\bar{c} = 0.1$. The phase lag is 90° for pressure

load case for $\omega/\omega_1 = 1$ and close to 90° for the potential load case. The amplitude $\bar{u}_m$ and phase lag $\kappa^\circ$ of the mid-surface deflection at the center of panel (d) with $S = 10$ are plotted in Fig. 5 as a function of $\omega/\omega_1$ for both load cases (1) and (2) for undamped ($\bar{c} = 0$) and damped ($\bar{c} = 0.1$) cases. The pattern of these response curves is very much similar to the case of a single degree of freedom system. The effect of ply-angle on central deflection is depicted in Figs. 6 and 7 for load cases (1) and (2), respectively, for hybrid angle-ply composite panel (c) for $\omega/\omega_1 = 0.7$, $\bar{c} = 0.1$ and $S = 5, 10$. The steady-state amplitude of deflection increases with the increase in ply-angle in both load cases. The increase is more for the pressure load case than for the potential load.

Table 4
Amplitude and phase of central deflection of panels under harmonic pressure load.

| Panel | $S$ | $\frac{\omega}{\omega_1} = 0.7$ | | | $\frac{\omega}{\omega_1} = 1$ | |
|---|---|---|---|---|---|---|
| | | $\bar{c} = 0$ | $\bar{c} = 0.1$ | | $\bar{c} = 0.1$ | |
| | | $\bar{u}_m$ | $\bar{u}_m$ | $\kappa^\circ$ | $\bar{u}_m$ | $\kappa^\circ$ |
| a | 5 | 0.80486 | 0.77847 | 14.71 | 2.1479 | 90.00 |
| | 10 | 2.8994 | 2.8082 | 14.41 | 7.9002 | 90.00 |
| | 20 | 11.149 | 10.810 | 14.18 | 30.896 | 90.00 |
| b | 5 | 0.63701 | 0.62569 | 10.82 | 2.3447 | 90.00 |
| | 10 | 0.33614 | 0.33045 | 10.56 | 1.2631 | 90.00 |
| | 20 | 0.25663 | 0.25243 | 10.39 | 0.97987 | 90.00 |
| c | 5 | 0.73808 | 0.72487 | 10.85 | 2.7054 | 90.00 |
| | 10 | 0.46959 | 0.46159 | 10.59 | 1.7591 | 90.00 |
| | 20 | 0.39717 | 0.39064 | 10.40 | 1.5149 | 90.00 |
| d | 5 | 1.8384 | 1.8169 | 8.78 | 8.3655 | 90.00 |
| | 10 | 0.78399 | 0.77544 | 8.47 | 3.6875 | 90.00 |
| | 20 | 0.51445 | 0.50903 | 8.32 | 2.4612 | 90.00 |

Table 5
Amplitude and phase of central deflection of panels under harmonic potential load.

| Panel | $S$ | $\frac{\omega}{\omega_1} = 0.7$ | | | $\frac{\omega}{\omega_1} = 1$ | |
|---|---|---|---|---|---|---|
| | | $\bar{c} = 0$ | $\bar{c} = 0.1$ | | $\bar{c} = 0.1$ | |
| | | $\bar{u}_m$ | $\bar{u}_m$ | $\kappa^\circ$ | $\bar{u}_m$ | $\kappa^\circ$ |
| a | 5 | 3.5336 | 3.4178 | 15.69 | 9.6472 | 91.34 |
| | 10 | 1.9424 | 1.8813 | 14.65 | 5.3621 | 90.34 |
| | 20 | 0.99631 | 0.96596 | 14.24 | 2.7800 | 90.09 |
| b | 5 | 0.64458 | 0.63314 | 10.44 | 2.3101 | 89.45 |
| | 10 | 0.57120 | 0.56153 | 10.47 | 2.1222 | 89.86 |
| | 20 | 0.54769 | 0.53870 | 10.37 | 2.0799 | 89.96 |
| c | 5 | 0.70113 | 0.68862 | 10.51 | 2.5260 | 89.52 |
| | 10 | 0.62444 | 0.61381 | 10.50 | 2.3202 | 89.88 |
| | 20 | 0.60096 | 0.59108 | 10.38 | 2.2832 | 89.97 |
| d | 5 | 1.2034 | 1.1893 | 8.57 | 5.2879 | 89.68 |
| | 10 | 1.0911 | 1.0791 | 8.43 | 5.0455 | 89.93 |
| | 20 | 1.0598 | 1.0486 | 8.32 | 5.0251 | 89.98 |

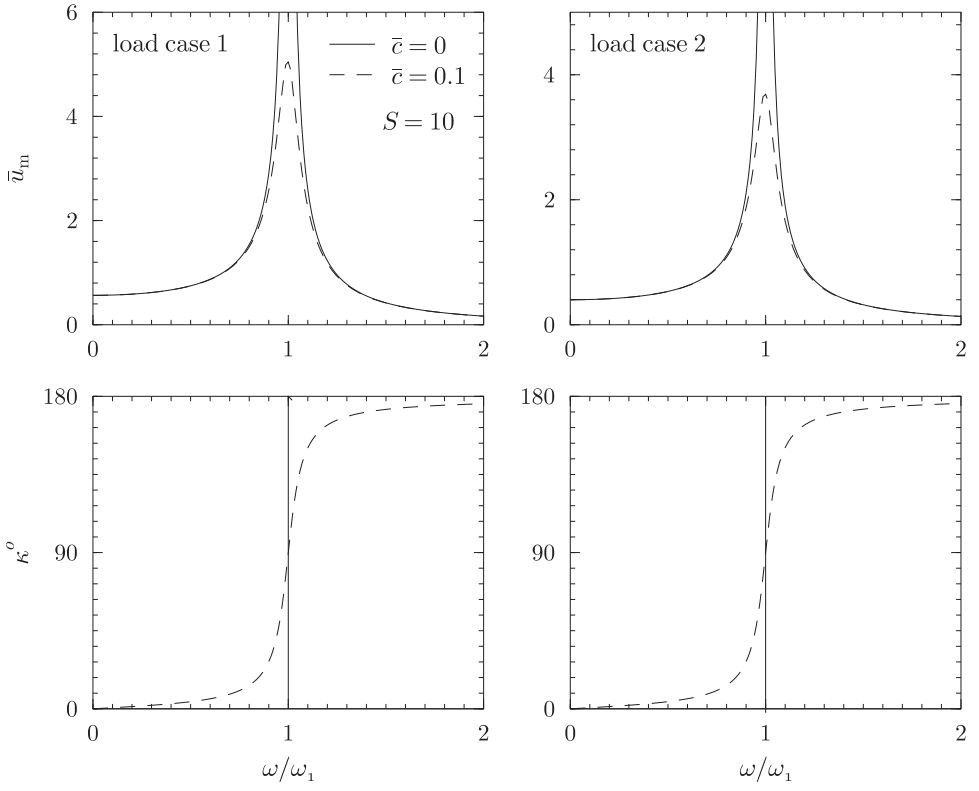


Fig. 5. Amplitude $\bar{u}_m$ and phase $\kappa^{\circ}$ for hybrid sandwich panel (d) under load cases (1) and (2).

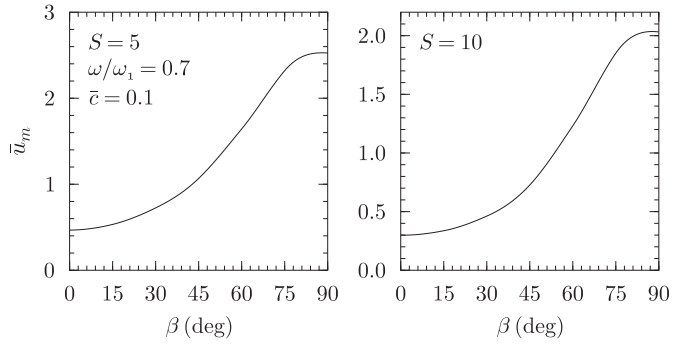


Fig. 6. Effect of ply-angle on central deflection amplitude of hybrid panel (c) for harmonic pressure load.

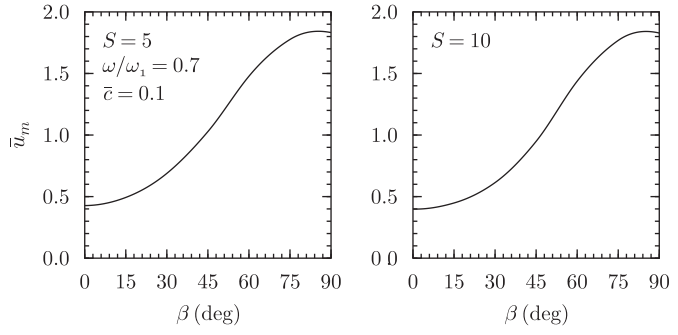


Fig. 7. Effect of ply-angle on central deflection amplitude of hybrid panel (c) for harmonic potential load.

The through-the-thickness distributions of dimensionless amplitude of deflection $\bar{u}$, inplane stress $\bar{\sigma}_\theta$ and transverse stress $\bar{\tau}_{r\theta}$ are shown in Figs. 8–10 for panels (b), (c) and (d) for both load cases (1) and (2) considering $\omega/\omega_1 = 0.7$ and $\bar{c} = 0.1$. It is observed that the distribution of $\bar{u}$ across the thickness is nonuniform especially for the potential load case (2). The distribution of the inplane stress $\bar{\sigma}_\theta$ becomes nonlinear across some layers for thick panels with $S = 5$.

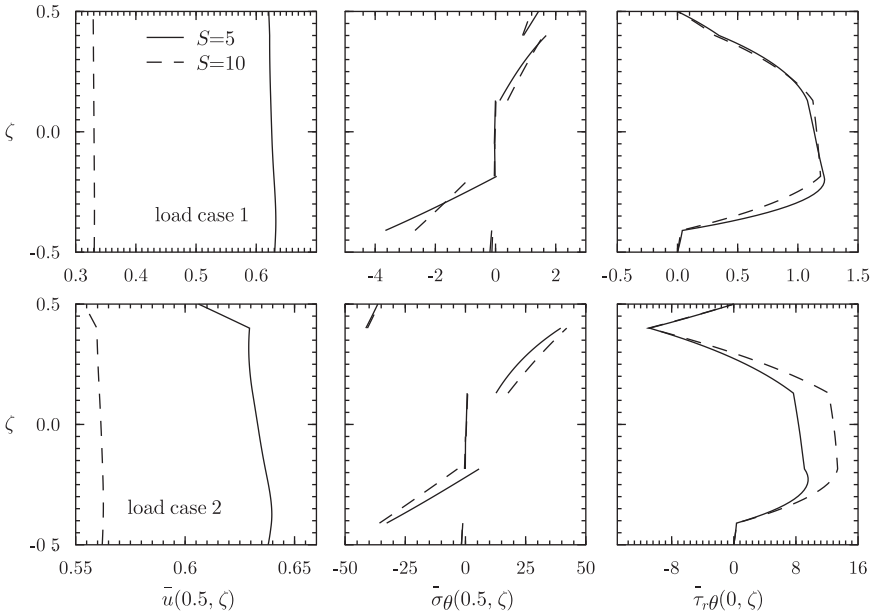


Fig. 8. Distributions of steady-state amplitudes of $\bar{u}$, $\bar{\sigma}_\theta$ and $\bar{\tau}_{r\theta}$ for hybrid test panel (b) under harmonic pressure and potential loading.

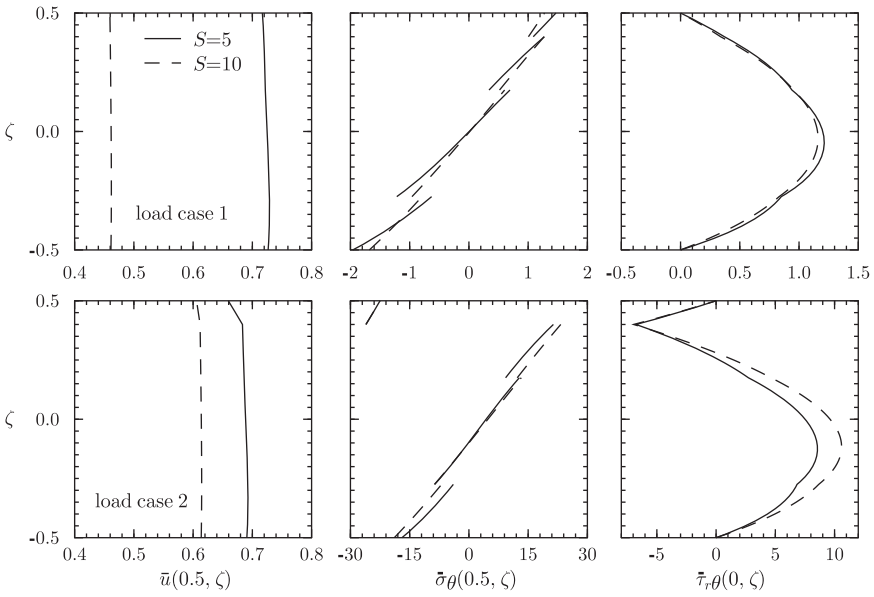


Fig. 9. Distributions of steady-state amplitudes of $\bar{u}$, $\bar{\sigma}_\theta$ and $\bar{\tau}_{r\theta}$ for hybrid composite panel (c) under harmonic pressure and potential loading.

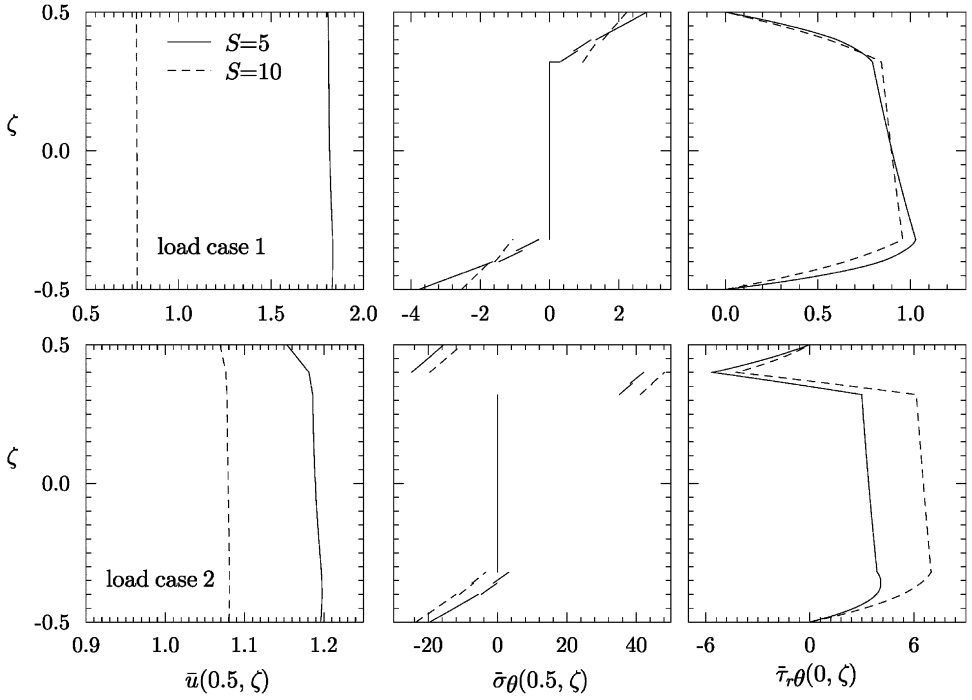


Fig. 10. Distributions of steady-state amplitudes of $\bar{u}$, $\bar{\sigma}_\theta$ and $\bar{\tau}_{r\theta}$ for hybrid sandwich panel (d) under harmonic pressure and potential loading.

## 6. Conclusions

An exact 2D piezoelasticity solution for free vibration and damped harmonic forced vibration response has been presented for simply supported hybrid piezoelectric angle-ply shell panels. Benchmark numerical results are presented for the natural frequencies and steady-state harmonic response of a piezoelectric panel, and hybrid angle-ply test, composite and sandwich panels. These results presented in tabular form will serve as useful benchmark against which the accuracy of 1D theories and approximate 2D solutions of hybrid angle-ply panels can be assessed. The change in the difference between OC and CC natural frequencies with thickness parameter and flexural mode number follows different trends for piezoelectric panels and hybrid panels. The increase in steady-state deflection amplitude with ply-angle is larger for pressure load than for the potential load.

## References

[1] H.J. Ding, W.Q. Chen, *Three Dimensional Problems of Piezoelasticity*, Nova Science Publisher, New York, 2001.
[2] P. Heyliger, Exact solution for simply supported laminated piezoelectric plates, *Journal of Applied Mechanics* 64 (1997) 299–306.
[3] J.S. Lee, L.Z. Jiang, Exact electroelastic analysis of piezoelectric laminae via state space approach, *International Journal of Solids and Structures* 33 (1996) 977–990.
[4] K. Xu, A.K. Noor, Y.Y. Tang, Three-dimensional solutions for coupled thermoelectroelastic response of multilayered plates, *Computer Methods in Applied Mechanics and Engineering* 126 (1995) 355–371.
[5] S. Kapuria, P.C. Dumir, S. Sengupta, Three-dimensional solution for shape control of a simply supported rectangular hybrid plate, *Journal of Thermal Stresses* 22 (1999) 159–176.
[6] P. Heyliger, D.A. Saravanos, Exact free-vibration analysis of laminated plates with embedded piezoelectric layers, *Journal of the Acoustical Society of America* 98 (1995) 1547–1557.
[7] S. Kapuria, G.G.S. Achary, Exact 3D piezoelasticity solution of hybrid cross-ply plates with damping under harmonic electromechanical loads, *Journal of Sound and Vibration* 282 (2005) 617–634.

[8] S. Kapuria, G.G.S. Achary, Exact 3D piezoelasticity solution for buckling of hybrid cross-ply plates using transfer matrices, *Acta Mechanica* 170 (2004) 25–45.
[9] G.P. Dube, M.M. Upadhyay, P.C. Dumir, S. Kapuria, Piezothermoelastic solution for angle-ply laminated plate in cylindrical bending, *Structural Engineering and Mechanics* 6 (1998) 529–554.
[10] P. Kumari, J.K. Nath, P.C. Dumir, S. Kapuria, 2D exact solutions for flat hybrid piezoelectric and magnetoelastic angle-ply panels under harmonic load, *Smart Materials and Structures* 16 (2007) 1651–1661.
[11] C.Q. Chen, Y.P. Shen, X.M. Wang, Exact solution of orthotropic cylindrical shell with piezoelectric layers under cylindrical bending, *International Journal of Solids and Structures* 33 (1996) 4481–4494.
[12] G.P. Dube, S. Kapuria, P.C. Dumir, Exact piezothermoelastic solution of simply-supported orthotropic circular cylindrical panel in cylindrical bending, *Archive of Applied Mechanics* 66 (1996) 537–554.
[13] S. Kapuria, P.C. Dumir, S. Sengupta, Exact piezothermoelastic axisymmetric solution of a finite transversely isotropic cylindrical shell, *Computers and Structures* 61 (1996) 1085–1099.
[14] H.J. Ding, R.Q. Xu, W.Q. Chen, Free vibration of transversely isotropic piezoelectric circular cylindrical panels, *International Journal of Mechanical Sciences* 44 (2002) 191–206.
[15] C.Q. Chen, Y.P. Shen, Piezothermoelasticity analysis for circular cylindrical shell under the state of axisymmetric deformation, *International Journal of Engineering Science* 34 (1996) 1585–1600.
[16] C.Q. Chen, Y.P. Shen, Three-dimensional analysis for free vibration of finite-length orthotropic piezoelectric circular cylindrical shells, *Transactions of the ASME Journal of Vibration and Acoustics* 120 (1998) 194–198.
[17] S. Kapuria, S. Sengupta, P.C. Dumir, Three-dimensional solution for a hybrid cylindrical shell under axisymmetric thermoelectric load, *Archive of Applied Mechanics* 67 (1997) 320–330.
[18] S. Kapuria, S. Sengupta, P.C. Dumir, Three-dimensional piezothermoelastic solution for shape control of cylindrical panel, *Journal of Thermal Stresses* 20 (1997) 67–85.
[19] K. Xu, A.K. Noor, Three-dimensional analytical solution for coupled thermoelectroelastic response of multilayered cylindrical shell, *American Institute of Aeronautics and Astronautics Journal* 34 (1996) 802–812.
[20] P.C. Dumir, G.P. Dube, S. Kumar, Piezothermoelastic solution for angle-ply laminated cylindrical panel, *Journal of Intelligent Material Systems and Structures* 8 (1997) 452–464.
[21] W.Q. Chen, K.Y. Lee, State-space approach for statics and dynamics of angle-ply laminated cylindrical panels in cylindrical bending, *International Journal of Mechanical Sciences* 47 (2005) 374–387.
[22] W.Q. Chen, J.P. Jung, K.Y. Lee, Static and dynamic behaviour of simply-supported cross-ply laminated piezoelectric cylindrical panels with imperfect bonding, *Composite Structures* 74 (2006) 265–276.
[23] Y. Ootao, Y. Tanigawa, Transient piezothermoelasticity for a cylindrical composite panel composed of angle-ply and piezoelectric laminae, *International Journal of Solids and Structures* 39 (2002) 5737–5752.
[24] W.Q. Chen, K.Y. Lee, Benchmark solution of angle-ply piezoelectric-laminated cylindrical panels in cylindrical bending with weak interfaces, *Archive of Applied Mechanics* 74 (2005) 466–476.
[25] E. Kreyszig, *Advanced Engineering Mathematics*, eighth ed., Wiley India (P) Ltd., New Delhi, 1999.